Sting jets in intense winter North-Atlantic windstorms

Oscar Martínez-Alvarado[1], Suzanne L Gray[1], Jennifer L Catto[2] and Peter A Clark[1]‡

[1] Joint Centre for Mesoscale Meteorology, Department of Meteorology, University of Reading, UK

[2] School of Geography and Environmental Science Monash University, VIC 3800, Australia

E-mail: `o.martinezalvarado@reading.ac.uk`

Abstract. Extratropical cyclones dominate autumn and winter weather over western Europe. The strongest cyclones, often termed windstorms, have a large socio-economic impact due to the strong surface winds and associated storm surges in coastal areas. Here we show that sting jets are a common feature of windstorms; up to a third of the 100 most intense North Atlantic winter windstorms over the last two decades satisfy conditions for sting jets. The sting jet is a mesoscale descending airstream that can cause strong near-surface winds in the dry slot of the cyclone, a region not usually associated with strong winds. Despite their localized transient nature these sting jets can cause significant damage, a prominent example being the storm that devastated southeast England on 16 October 1987. We present the first regional climatology of windstorms with sting jets. Previously analysed sting jet cases appear to have been exceptional in their track over northwest Europe rather than in their strength.

PACS numbers: 92.60.Qx, 92.60.Ry, 92.60.Wc

Keywords: high-resolution modelling; climatology; extratropical cyclones; ERA-Interim

‡ Present address: Departments of Mathematics and Civil, Chemical and Environmental Engineering, University of Surrey, Guildford, UK

1. Introduction

Worldwide, European windstorms are second only to United States hurricanes as a traded catastrophe risk (Browning 2004). While larger-scale aspects of extratropical cyclones are generally forecast with reasonable skill, the occurrence, location, and severity of the local regions of major wind damage are not. Two regions of strong low-level winds commonly occur during the passage of a cyclone. The warm conveyor belt is a broad region of moderately strong surface winds that exists throughout most of the cyclone's life cycle in the warm sector of the cyclone (to the south of the storm centre in the northern hemisphere). When the cyclone is mature the cold conveyor belt may also produce strong surface winds if it hooks around the cloud head that can be seen curving to the northwest around the storm centre. Additionally, a third localized region of strong winds, and especially strong gusts, which may be short lived (a few hours) can exist close to the 'tail' of the cloud head hook as it wraps around the cyclone centre. This has been dubbed the 'sting at the end of the tail', or 'sting jet', by Browning (2004), terminology similar to that used by Grønås (1995) who referred to a similar feature that he called the 'poisonous tail' of the bent-back occlusion.

Sting jets are defined as accelerating, drying airflows that descend from the cloud head in the mid-troposphere (beneath the dry intrusion) towards the top of the boundary layer while conserving wet-bulb potential temperature. The descent occurs in the frontal fracture region of cyclones that follow the Shapiro–Keyser (Shapiro & Keyser 1990) conceptual model (Browning 2004, Clark et al. 2005). This region is usually relatively clear of cloud and is hence known as the 'dry slot'. Sting-jet momentum can then be transferred from the top of the boundary layer to the surface via boundary-layer processes, such as turbulent mixing, generating strong surface winds and gusts; this momentum transfer may be promoted by the weak moist static stability in the frontal fracture region.

Despite their damage potential the frequency and global distribution of sting-jet cyclones are unknown. The limited published research on sting jets to date almost exclusively consists of analyses of case studies (Browning 2004, Browning & Field 2004, Clark et al. 2005, Martínez-Alvarado et al. 2010, Parton et al. 2009, Baker 2009). The one exception is a climatology of strong mid-tropospheric mesoscale winds observed by the vertically pointing Mesosphere–Stratosphere–Troposphere (MST) radar (Vaughan 2002) located near Aberystwyth, Wales (Parton et al. 2010). Nine potential sting-jet cases were identified in seven years, but this number only represents possible sting jet events passing over Aberystwyth. Their mesoscale nature (∼150 km across) means that sting jets are not resolved by operational weather forecast models with domains large-enough to cover storm-tracks. Nor are they represented in the even coarser resolution multi-year reanalysis datasets; hence wind climatologies based on these may miss the most damaging parts of windstorms. Furthermore, observational datasets do not provide sufficient temporal resolution over the oceans to allow exhaustive identification of these transient features.

To determine the climatological characteristics of sting-jet cyclones we have developed a method to diagnose the precursors of sting jets (rather than the unresolved sting jets themselves) from reanalysis datasets (Martínez-Alvarado et al. 2011). We search for conditional symmetric instability (CSI) in the moist frontal fracture zones of cyclones. The method is applied to the 100 most intense North-Atlantic cyclones during 20 winter seasons (December-January-February, DJF) of the European Centre for Medium-Range Weather Forecasts (ECMWF) reanalysis, ERA-Interim (Simmons et al. 2007). The predicted presence or absence of a sting jet is then verified by performing high-resolution, sting-jet resolving, simulations with the Met Office weather forecast model (Davies et al. 2005) for 15 randomly sampled cases.

2. Methods

2.1. Reanalysis data and cyclone tracks

ERA-Interim is a 6-hourly, global, gridded dataset of the state of the atmosphere consistent with both a numerical model derived from the operational ECMWF forecasting system (IFS Cy31r1/2) and observations via a 12-hour 4D-Var data assimilation cycle. In the horizontal direction the data used has been interpolated from the original T255 spectral resolution onto a regular latitude-longitude grid at the equivalent grid spacing of $0.7^\circ \times 0.7^\circ$. In the vertical direction it was interpolated from the original 60 model levels to pressure levels between 1000 hPa and 300 hPa, with a 25-hPa level separation between 1000 hPa and 750 hPa and a 50-hPa level separation elsewhere. Following the work by Catto et al. (2010), an objective feature tracking algorithm (Hodges 1994, Hodges 1995, Hodges 1999, Hoskins & Hodges 2002) has been applied to ERA-Interim. The tracks of the 100 most intense cyclones (with respect to 850-hPa relative vorticity truncated to T42 resolution to emphasize the synoptic scales) over the North Atlantic ocean during the winter seasons (DJF) from 1989/1990 to 2008/2009 have been identified.

2.2. Diagnostic for sting-jet precursor conditions

We applied a diagnostic designed to detect sting-jet precursor conditions in low-resolution datasets (Martínez-Alvarado et al. 2011) to each cyclone from 0000 UTC on the day before to 1800 UTC on the day after the day on which the maximum relative vorticity occurred. The diagnostic for sting-jet precursor conditions (Martínez-Alvarado et al. 2011) detects downdraught CSI as measured by downdraught slantwise convective available potential energy (DSCAPE) in the moist frontal fracture zone. The release of this CSI is a cause of sting jets and DSCAPE is present in cyclones with sting jets but not present in other, equally intense, cyclones that do not have sting jets (Gray et al. 2011). Insufficient model resolution does not prohibit the accumulation of CSI, only its realistic release to generate a sting jet (Martínez-Alvarado et al. 2011).

2.2.1. Definition of DSCAPE DSCAPE is defined as the potential energy available to a hypothetical air parcel for descent, while conserving absolute momentum, from a pressure-level $p_{\rm top}$ to a pressure-level $p_{\rm bottom}$, assuming that it becomes saturated through the evaporation of rain or snow falling into it from upper levels (Emanuel 1994). The pressure-levels $p_{\rm top}$ and $p_{\rm bottom}$ are prescribed: $p_{\rm top}$ is varied from 800 hPa to 450 hPa and $p_{\rm bottom}$ is kept constant, and equal to 950 hPa. Thus, DSCAPE is computed as

$$\mathrm{DSCAPE} = \int_{p_{\rm top}}^{p_{\rm bottom}} R_d\,(T_{v,e} - T_{v,p})\,d\ln p, \qquad (1)$$

where R_d is the dry air gas constant, p is pressure, $T_{v,p}$ is the parcel virtual temperature, and $T_{v,e}$ is the environmental virtual temperature. The integral in (1) is evaluated along a surface of constant vector absolute momentum in a similar way to that used for the calculation of SCAPE (Shutts 1990). The maximum value of DSCAPE (DSCAPE*) and associated value of $p_{\rm top}$ ($p^*_{\rm top}$) for a vertical column is used as a representative DSCAPE value for the underlying grid point.

2.2.2. Thresholds for diagnostic A minimum threshold for DSCAPE* is imposed but this is not sufficient to discriminate CSI regions that could generate sting jets. For example, there are often large amounts of DSCAPE in dry regions such as the cyclone dry slot; DSCAPE in these regions cannot be released due to the lack of moisture required to saturate air parcels and trigger their descent. Additional conditions are imposed to restrict the regions with CSI identified to only those that are cloudy and near a cold front (and so potentially near a frontal fracture zone). The following recommended thresholds (Martínez-Alvarado et al. 2011) are imposed on relative humidity, RH, the magnitude of the gradient of wet-bulb potential temperature, $|\nabla\theta_w|$, and cross-front θ_w-advection, $\mathbf{V}\cdot\nabla\theta_w$, where $\mathbf{V}$ is the horizontal wind vector:

$$\begin{cases} \mathrm{DSCAPE} & > & 200\ \mathrm{J\,kg^{-1}}, \\ \mathrm{RH} & > & 80\ \%, \\ |\nabla\theta_w| & > & 10^{-5}\ \mathrm{K\,m^{-1}}, \\ \mathbf{V}\cdot\nabla\theta_w & > & 10^{-4}\ \mathrm{K\,s^{-1}}. \end{cases} \qquad (2)$$

Mean values were used of θ_w and $\mathbf{V}$ over layers of 100 hPa depth centred around $p^*_{\rm top}$ (vertically delimited by pressure levels above and below $p^*_{\rm top}$). Maximum values of RH were used from within those same layers.

Further constraints, not included in Martínez-Alvarado et al. (2011), were imposed on the position, relative to cyclone centres, of precursor regions. Previous studies have shown that regions from which sting jets originate are typically located within a 300-km radius from a cyclone's pressure centre (e.g. Gray et al. 2011). In this study, the centre of a precursor region was required to lie within a radius of 700 km from the pressure-based cyclone position (in the full-resolution data and associated with the truncated T42 relative vorticity position) in order to be considered as a potential sting-jet precursor; this encompassed the whole cloud head. Precursor regions entirely in the sector between 300° and 100° relative to the direction of cyclone motion and beyond 250 km from the cyclone centre were discarded as these lay along the warm conveyor belt of the cyclone (CSI release may occur here but it will not lead to sting jets). Figure 1 shows a graphic description of these elements. The cloudy area (cloud head and warm conveyor belt) in that figure was defined by a 550-hPa relative humidity (RH > 80%) composite over every cyclone with CSI and every time instability was exhibited.

The size of the precursor region was defined by the number of connected grid columns in which a parcel descending from p^*_{top} satisfies the precursor conditions. To describe the shape and location of the average precursor region the central position of this region for each cyclone was computed in polar coordinates, taking radial and azimuthal position separately, relative to its direction of travel. The maximum upper and maximum lower deviations from the central position were then calculated in both the radial and azimuthal direction. These deviations were averaged over the precursor regions for all cyclones to obtain a representative shape considering possible asymmetries in the shape of the regions. In practice these asymmetries turned out to be small.

2.3. Verification of the presence of sting jets

In the absence of a suitable observational dataset, verification of the cyclones as having had or not having had a sting jet has been achieved by performing high-resolution, sting-jet resolving, simulations with the Met Office Unified Model (MetUM) (Davies et al. 2005). Fifteen cyclones drawn randomly from the 100 intense cyclones were simulated; the number was limited by computational cost but it is shown to be sufficient to demonstrate skill.

2.3.1. Numerical model The MetUM version 7.1 was used to perform the sting-jet resolving cyclone simulations. This is an operational finite-difference model that solves the non-hydrostatic deep-atmosphere dynamical equations with a semi-implicit, semi-Lagrangian integration scheme (Davies et al. 2005). It uses Arakawa C staggering in the horizontal (Arakawa & Lamb 1977) and is terrain following with a hybrid-height vertical coordinate and Charney–Phillips staggering (Charney & Phillips 1953) in the vertical. Parameterization of physical processes includes longwave and shortwave radiation (Edwards & Slingo 1996), boundary layer mixing (Lock et al. 2000), cloud microphysics and large-scale precipitation (Wilson & Ballard 1999), and convection (Gregory & Rowntree 1990).

The limited-area domain comprised 720 × 432 grid points (with a spacing of 0.11° ∼ 12 km), covering nearly all of the North Atlantic, Europe, and North Africa and 76 vertical levels (lid around 39 km, mid-tropospheric vertical spacing around 280 m). This vertical spacing yields a vertical to horizontal scale ratio of around 1:40, consistent with the ratio used by Clark et al. (2005) and resolution recommendations to resolve CSI release (Persson & Warner 1991, Persson & Warner 1993). Lateral boundary conditions were produced by running the MetUM in its global configuration. The global model was initialized using global ECMWF operational analyses (ECMWF cited 2010) obtained at a grid spacing of 0.25° and 60 vertical levels. These were interpolated to the global model resolution with 640 × 481 grid points (spacing 0.4° ∼ 40 km meridionally) and 50 vertical levels (lid around 60 km). The limited-area model was initialized by interpolating the initial conditions produced for the global model.

2.3.2. Detection of sting jets Sting jets were identified using a three-step method (Martínez-Alvarado et al. 2010): (a) localisation and clustering of near-surface sting jet points, (b) backward-trajectory analysis (Wernli & Davies 1997) and (c) analysis of the evolution of atmospheric variables along trajectories. At the end of their descent sting jets are here defined as low-level strong, descending winds in a relatively dry region within the frontal-fracture zone hence meeting the criteria $|\mathbf{V}| > 35\ \mathrm{m\,s^{-1}}$, $w < -0.05\ \mathrm{m\,s^{-1}}$, RH < 80 %, and $\theta_{w,\mathrm{min}} < \theta_w < \theta_{w,\mathrm{max}}$ where w is vertical velocity. The θ_w values delimiting the frontal region, $\theta_{w,\mathrm{min}}$ and $\theta_{w,\mathrm{max}}$, have been set on a case-by-case basis. Clusters of points satisfying these criteria were identified and backward trajectories from these clusters computed.

Relative humidity, pressure and θ_w were computed along trajectories to determine if they descended from a cloudy region (i.e. the cloud head) while conserving θ_w. Specific humidity and θ were computed along trajectories to determine if evaporative cooling contributed to their descent. Saturated moist potential vorticity (MPV*), absolute vorticity (as a measure of inertial instability, and defined as $\zeta_a = f + \xi$, where f is the Coriolis parameter and ξ is relative vorticity) and moist static stability (N_m^2) (Durran & Klemp 1982) as a measure of gravitational instability of a saturated atmosphere were computed along trajectories to assess CSI.

3. Results

3.1. Sting-jet cyclone characteristics

The number of cyclones with a sting-jet precursor is dependent on a threshold used for the minimum size of the precursor region (defined by the number of connected grid columns in which the diagnostic is satisfied where the area of one grid box is $\sim 4000\ \mathrm{km}^2$). This was optimized using the cases verified by high-resolution modelling and the skill of the precursor diagnostic is inferred from 2×2 contingency table (table 1) relating the presence or absence of a precursor to the presence or absence of a sting jet. Six of the fifteen cases simulated at high resolution developed trajectories consistent with the definition of a sting jet. If the minimum size threshold was set to between five and eight grid columns inclusive then five of the six sting-jet cases had precursor regions and seven of the nine cases without sting jets did not have precursor regions. The precursor diagnostic has skill for these size thresholds as this yields a p-value of 0.035 using Fisher's exact test; other size thresholds yield p-values above 0.05 (i.e. the 95% significance level). For minimum size thresholds yielding significant verification results, between 23 and 32 of the 100 cyclones had sting-jet precursor regions. Analysis is now presented of the maximum possible number of sting jet cyclones, i.e. using a minimum precursor region size of five grid columns.

The analysed portions of the cyclone tracks are mapped every six hours for the cyclones with and without sting-jet precursors in figures 2a and b respectively. Sting-jet precursors occurred only once for most of the tracks (69%) though there were tracks with two (16%), three (12%) and five (3%) precursor occurrences possibly suggesting multiple sting jets. The precursor regions occurred throughout the North Atlantic. The analysed tracks follow the classical North Atlantic storm track (Hoskins & Hodges 2002). However, a difference between the start locations of the analysed tracks with and without sting-jet precursors exists: those with sting-jet precursors all originated south of 50°N whereas those without originated as far north as 65°N. This may be indicative of a requirement for a warm moist airmass where these cyclones form, consistent with the known importance of diabatic processes in the generation of sting jets. There is a strong tendency for the sting-jet precursors to occur in the 30 hours prior to the occurrence of the cyclone's maximum intensity (figure 2c). This is consistent with the sting-jet conceptual model in which sting jets occur during frontal fracture in stages II and III of the evolution of cyclones following the Shapiro–Keyser (Shapiro & Keyser 1990) conceptual model (Clark et al. 2005).

The frequency distribution of the maximum relative vorticity of all of the 100 most intense North Atlantic cyclones, and just those with sting-jet precursors, shows that there are fewer cyclones with increasing vorticity as expected (figure 3a, note that the first vorticity bin contains relatively few cyclones because other cyclones with vorticity in this range are not among the 100 most intense). Sting-jet precursors occur in cyclones throughout the vorticity range. The 100 most intense cyclones are relatively evenly distributed over the 20 winter seasons (figure 3b) with between 2 and 10 of these cyclones occurring in each season; between 0 and 3 of these cyclones have sting-jet precursors each year. Recent studies have found contradictory results regarding long-term trends in the frequency and intensity of extreme cyclones in the second half of the 20$^{\text{th}}$ century (e.g. Ulbrich et al. 2009). Statistically significant trends cannot be inferred from the limited data presented here; however, we note that the three winter seasons in which there were no sting-jet cyclones all occurred during the last six seasons analysed.

The locations of sting-jet precursors are shown in a system-relative reference frame in figure 4a. Each precursor region has been rotated such that the direction of motion of the cyclone is orientated to the right. The dots represent the locations of the gridpoints within every precursor region relative to the corresponding cyclone centre. There are gridpoints in areas apparently restricted (warm conveyor belt area in figure 1). However, these gridpoints belong to precursor regions lying at least partly within the permitted area (cloud head area in figure 1). The gridpoints span the space to the west of the cyclone centre where the cloud head lies (*cf.* figures 10b and d of Catto et al. (2010) which show relative humidity from composite cyclones). The average precursor region (computed following the method described in section 2.2.2) lies between 279 km and 536 km radially (mean at 400 km) and 154° and 223° azimuthally (mean at 186°).

This region is shaded in figure 4a and yields an area of 126×10^3 km^2. The precursor location is consistent with the origin locations of sting jets in previous studies (Gray et al. 2011, Martínez-Alvarado et al. 2011) (although these regions are all within 300 km of the cyclone centre in these studies) and with the bands of updraught CSI found in the cloud head of the sting-jet windstorm Jeanette (Parton et al. 2009).

The maximum energy available to the descending sting jet through the release of CSI, measured by maximum downdraught slantwise convective available potential energy in an atmospheric column (DSCAPE*), ranges from the minimum threshold considered (200 J kg^{-1}) to 900 J kg^{-1} with a mode of 300–350 J kg^{-1} (figure 4b). The pressure level from which the descending jet has this maximum energy (p^*_{top}) is typically above 650 hPa (90% of cases) with many cases at 450 hPa, which constitutes the lowest pressure considered (figure 4b). These results imply that the identification of sting-jet precursor regions is sensitive to these thresholds for energy and pressure and that a definitive sting-jet precursor cannot be defined.

3.2. Sting jet characteristics

The characteristics of sting jets found by applying trajectory analysis to the high-resolution model output are now described. The evolution of pressure, relative humidity and saturated moist potential vorticity (MPV*) along one ensemble of sting-jet trajectories from each cyclone are shown in figure 5. More than one ensemble of trajectories satisfying the criteria for a sting jet was found in some cyclones, those illustrated are chosen because they descend for similar periods and have comparable ensemble sizes. The trajectories are plotted over the 10 hours prior to the time at which they reach their lowest level in the atmosphere; the vertical lines mark the onset of the sting-jet descent from the mid-troposphere towards the top of the boundary layer (the transport of momentum from here to the surface by parameterized processes in the model cannot be diagnosed from trajectories calculated using the model-resolved winds). The one false-negative case (for which a sting-jet precursor was not identified) was the cyclone of 12 December 1994 (bottom row in figure 5). The ensemble-mean trajectory descent rate ranges from $\omega = 0.4$ to 0.9 Pa s^{-1} which compares well to previous studies (0.5, 0.8, and 1.3 Pa s^{-1} for windstorms Gudrun and Anna and the Great October storm respectively (Gray et al. 2011)). However, the true-positive cases achieve this descent rate for a minimum of 5 hr compared to just 2 hr for the false-negative case. The false-negative case is also distinct in that it remains at low-levels throughout its development (below the 700 hPa level). The transition from cloudy air to dry air after the onset of descent is shown in the decrease in relative humidity for all cases. The ensemble-mean horizontal wind speed at the end of the trajectories ranges from 36 to 43 m s^{-1} (not shown) which also compares well to previous studies (42, 35–37 (values from two different models), and 48 m s^{-1} for windstorms Gudrun (Baker 2011), Anna (Martínez-Alvarado et al. 2010) and the Great October storm (Clark et al. 2005) respectively).

The existence of negative MPV*, but static and inertial stability, along a moist descending trajectory implies that CSI is being released. Each sting jet has at least some trajectories satisfying these criteria and, in all but the case of 26 December 1998, the mean MPV* is close to zero throughout almost all of the period shown (figure 5c); almost all ensemble members were statically and inertially stable (not shown). Further analysis of the case of 26 December 1998 revealed that the low-level strong winds in the frontal fracture region were the result of two different airstreams merging together at upper levels. The first stream approached the cyclone centre from the south-west at upper levels and had negative MPV*; this was the sting jet. The second stream was a frontal circulation rising cyclonically around the cyclone centre and had partially negative MPV* at lower levels that became positive as it ascended; this stream could be releasing CSI as it ascends in the frontal circulation. As the streams met, MPV* became negative in some of the upper-level trajectory parcels, while lower-level ones experienced an increase in the value of MPV*. This merging of different airstreams has been observed previously in a sting jet storm (windstorm Anna (Martínez-Alvarado et al. 2010)) suggesting it could be a common occurrence. In windstorm Anna the sting jet was of similar size (defined by the number of trajectories) to the frontal circulation, whereas in the 26 December 1998 case the sting jet was much smaller than the frontal circulation.

4. Discussion and conclusions

The first regional climatology of sting-jet cyclones has been produced by applying a recently developed method for diagnosing sting-jet precursor regions in models incapable of resolving the sting jets themselves. The method has been applied to the 100 most intense extratropical cyclones that occurred in winter in the North Atlantic region between 1989 and 2009. The method is demonstrated to have skill by performing high-resolution sting-jet resolving weather forecasts of a sample of the cyclones.

Between 23 and 32% of the cyclones examined satisfied the diagnostic for the sting-jet precursor (dependent on the minimum area threshold chosen for the precursor region). The diagnostic depends on thresholds chosen to define the moist frontal fracture region (in which sting jets occur), the minimum energy available to be released from a type of atmospheric instability associated with sting jets and the highest pressure level from which the sting jet can descend. Consistent with previous work, these results imply that these thresholds are somewhat arbitrary; features consistent with the definition of sting jets exist for a spectrum of available energies and descent levels. It is left to future work to determine the relationship between these variables and the strength of the resultant sting jet (measured by metrics such as surface winds, top of boundary-layer winds, sting-jet extent etc.).

The sting-jet precursor regions cover most of the area corresponding to the southern edge of the cloud head of the storm that curves around the storm centre to the northwest; it is from the cloud head tip that the sting jet emanates. The precursor regions occur along the entire North Atlantic storm track. However, the first points in the analysed track sections (which occur the day before the time of maximum intensity of the cyclones) are skewed to the south for cyclones with sting-jet precursors, relative to the entire set of cyclones. This is indicative of the requirement for warm moist air to fuel the diabatic processes that generate sting jets. Consistent with previous case studies the precursors preferentially occur prior to the time when the cyclone reaches its maximum intensity.

Trajectories calculated along the sting jets in the high-resolution simulations demonstrate the expected characteristics of sting jets. In particular, CSI is released in the descending sting jet. The sting-jet descent rates and peak horizontal wind speeds at the top of the boundary layer compare well with previously analysed case studies. These results suggest that sting jets are a relatively generic feature of North Atlantic cyclones and that previously analysed sting jet cyclones are more exceptional in their path over populated areas (which led to their identification as sting-jet storms) than in the strength of their sting jets. We also note that the Great October storm was exceptional in both its path and its strength (not matched by any of the high-resolution simulated cyclones discussed here).

These results have potential impact for end-users including the insurance/re-insurance industry, policy makers and engineers responsible for the design of infra-structure subject to wind load (Baker 2007). More research is needed to determine the relationship between metrics for the existence of sting jets (such as the instability-based diagnostic applied here) and the strength of the associated observed surface winds and gusts.

Acknowledgements

This work has been funded by the Natural Environment Research Council (NERC) through the grant NE/E004415/1. The authors thank ECMWF for providing ERA-Interim, the Met Office for making the Met Office Unified Model available, and the NERC-funded NCAS (National Centre for Atmospheric Sciences) CMS (Computational Modelling Services) for providing computing and technical support.

References

Arakawa A & Lamb V 1977 *Methods Comput. Phys.* **17**, 173–265.
Baker C 2007 *J. Wind. Eng. Ind. Aerodyn.* **95**, 843–870.
Baker L 2009 *Weather* **64**, 143–148.
Baker L 2011 Sting jets in extratropical cyclones PhD thesis University of Reading.
Browning K A 2004 *Q. J. Roy. Meteor. Soc.* **130**, 375–399.
Browning K A & Field M 2004 *Meteorol. Appl.* **11**, 277–289.
Catto J L, Shaffrey L C & Hodges K L 2010 *J. Climate* **23**, 1621–1635.
Charney J G & Phillips N A 1953 *J. Meteor.* **10**(2), 71–99.
Clark P A, Browning K A & Wang C 2005 *Quart. J. Roy. Meteor. Soc.* **131**, 2263–2292.

Davies T, Cullen M J P, Malcolm A J, Mawson M H, Staniforth A, White A A & Wood N 2005 *Q. J. Roy. Meteor. Soc.* **131**, 1759–1782.

Durran D R & Klemp J B 1982 *J. Atmos. Sci.* **39**, 2152–2158.

ECMWF cited 2010 'ECMWF operational analysis data'. Available online from the British Atmospheric Data Centre. 2006– at http://badc.nerc.ac.uk/data/ecmwf-op/.

Edwards J & Slingo A 1996 *Q. J. Roy. Meteor. Soc.* **122**, 689–719.

Emanuel K A 1994 *Atmospheric convection* Oxford University Press.

Gray S L, Martínez-Alvarado O, Baker L H & Clark P A 2011 *Q. J. Roy. Meteor. Soc.* **137**, 1482–1500.

Gregory D & Rowntree P R 1990 *Mon. Weather Rev.* **118**, 1483–1506.

Grønås S 1995 *Tellus* **47A**, 733–746.

Hodges K I 1994 *Mon. Weather Rev.* **122**, 2573–2586.

Hodges K I 1995 *Mon. Weather Rev.* **123**, 3458–3465.

Hodges K I 1999 *Mon. Weather Rev.* **127**, 1362–1373.

Hoskins B J & Hodges K I 2002 *J. Atmos. Sci.* **59**, 1041–1061.

Lock A P, Brown A R, Bush M R, Martin G M & Smith R N B 2000 *Mon. Wea. Rev* **128**, 3187–3199.

Martínez-Alvarado O, Gray S L, Clark P A & Baker L H 2011 Objective detection of sting jets in low-resolution atmospheric datasets. *Meteorol. Appl.* In Press.

Martínez-Alvarado O, Weidle F & Gray S L 2010 *Mon. Weather Rev.* **138**, 4054–4075.

Parton G A, Dore A & Vaughan G 2010 *Meteorol. Appl.* .

Parton G A, Vaughan G, Norton E G, Browning K A & Clark P A 2009 *Q. J. Roy. Meteor. Soc.* **135**, 663–680.

Persson P O G & Warner T T 1991 *Mon. Weather Rev.* **119**, 917–935.

Persson P O G & Warner T T 1993 *Mon. Weather Rev.* **121**, 1821–1833.

Shapiro M A & Keyser D 1990 *in* C. W Newton & E. O Holopainen, eds, 'Extratropical cyclones: The Erik Palmén Memorial Volume' American Meteorological Society Boston, USA pp. 167–191.

Shutts G J 1990 *Mon. Weather Rev.* **118**, 2745–2751.

Simmons A J, Uppala S, Dee D & Kobayashi S 2007 *ECMWF Newsletter* **110**, 25–35.

Ulbrich U, Leckebusch G C & Pinto J G 2009 *Theor. Appl. Climatol.* **96**, 117–131.

Vaughan G 2002 *Weather* **57**, 69–73.

Wernli H & Davies H C 1997 *Q. J. Roy. Meteor. Soc.* **123**, 467–489.

Wilson D R & Ballard S P 1999 *Q. J. Roy. Meteor. Soc.* **125**, 1607–1636.

Table 1: 2×2 contingency table after fifteen cases. Minimum size of region is 5–8 grid columns inclusive. The p-value, $p = 0.035$, was calculated using the Fisher exact probability test.

	Sting jet	No sting jet	Totals
Sting jet precursor	5	2	7
No precursor	1	7	8
Totals	6	9	15

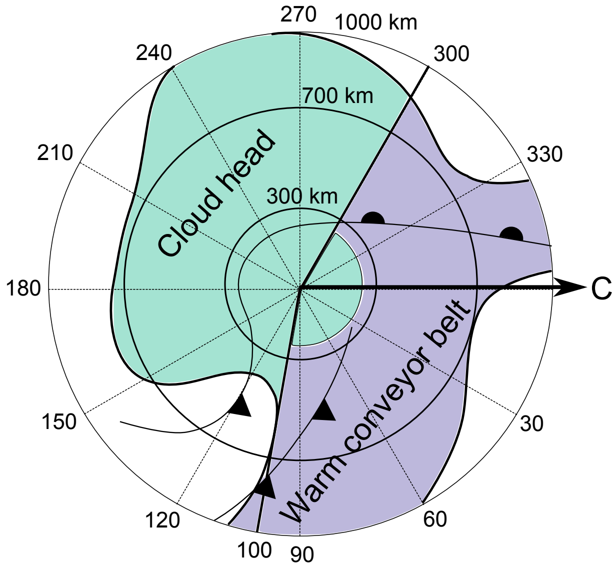

Figure 1: Cyclone elements relevant to the detection of sting-jet precursors. The pressure-based cyclone centre is located at the origin of coordinates. The black line represents a contour of cloudy air. The shaded regions show the definition of cloud head and warm conveyor belt for this purpose. The surface fronts are marked following the usual convention. Their position is only indicative. The axis C indicates the cyclone's direction of travel. See text for details.

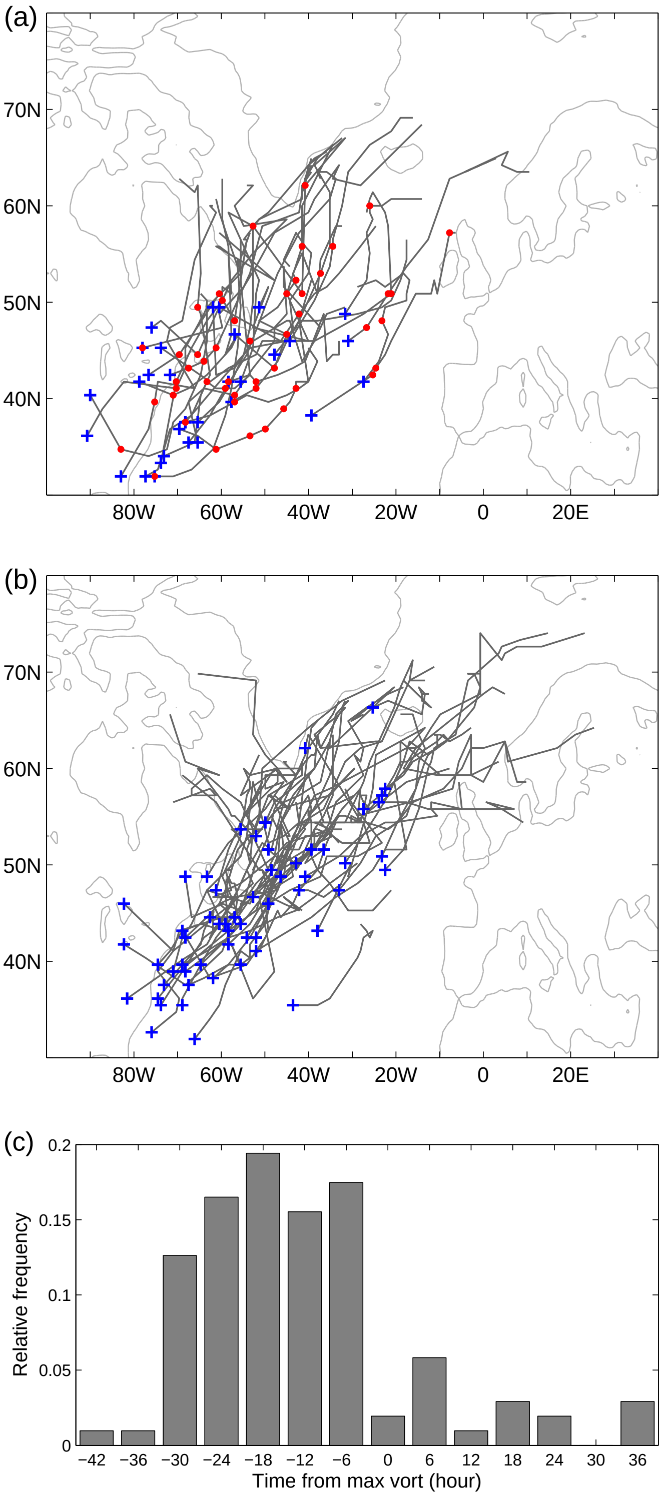

Figure 2: Track sections plotted every 6 hrs from 0000 UTC the day before to 1800 UTC the day after the day of maximum relative vorticity (at 850-hPa truncated to T42 resolution) for cyclones (a) with and (b) without sting-jet precursors. The start of the track sections are marked by a cross (+). The track points at which sting-jet precursors were identified are marked by a dot (.) in (a). (c) Distribution of sting-jet precursors with respect to the time of maximum relative vorticity.

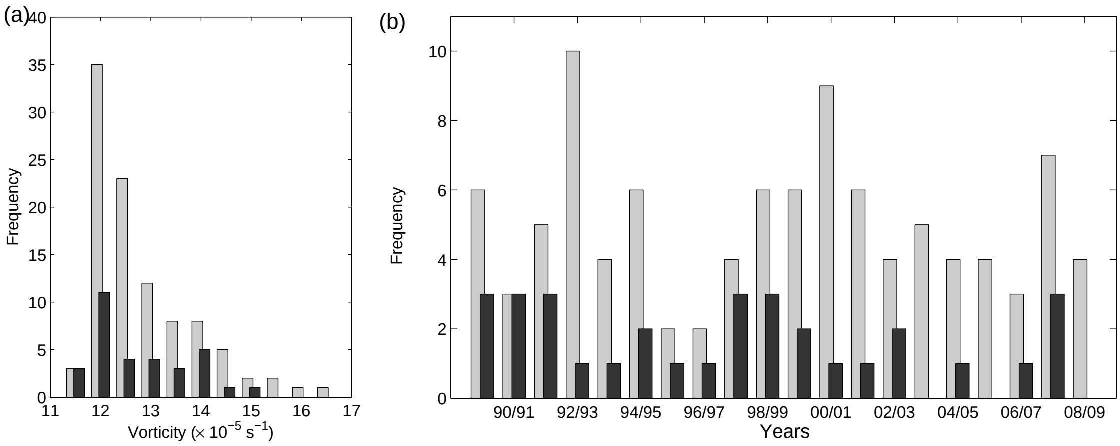

Figure 3: (a) Maximum relative vorticity distribution of all cyclones (grey) and those cyclones with sting-jet precursors (black). Bin width is 0.5×10^{-5} s^{-1}; bin centres start at 11.5×10^{-5} s^{-1} and finish at 16.5×10^{-5} s^{-1}. (b) Time distribution (by year) of all cyclones (grey) and those with sting-jet precursors (black). The 100 most intense cyclones in the North Atlantic during winter months from December 1989 to February 2009 are considered.

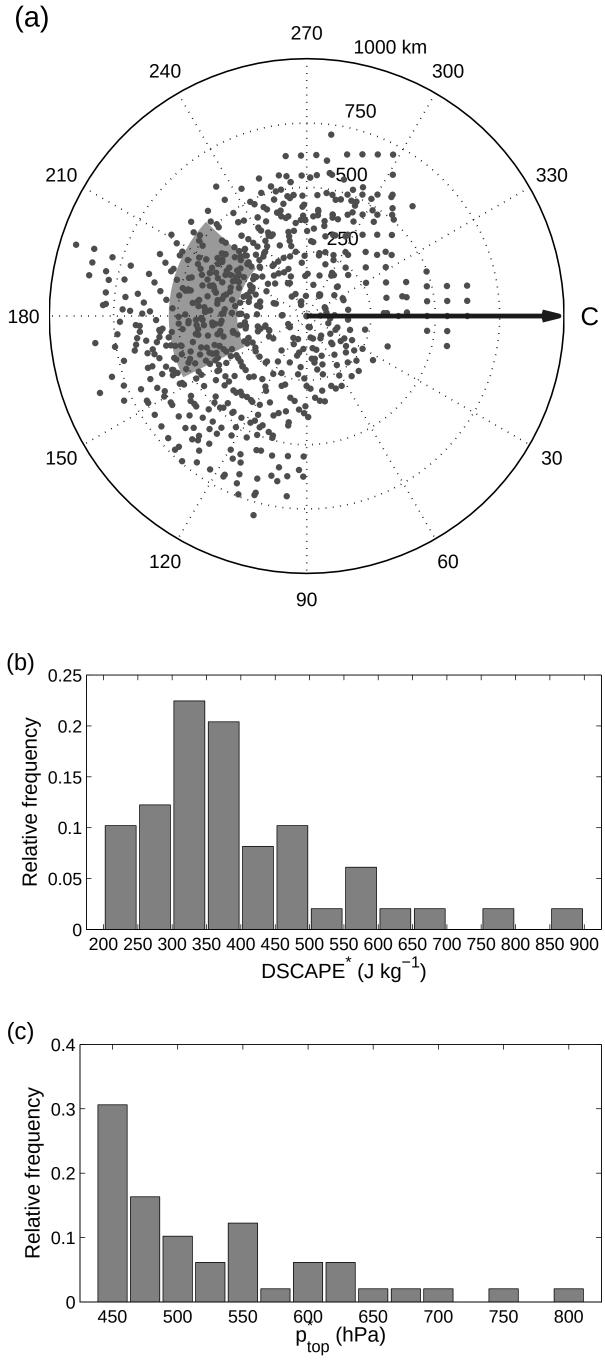

Figure 4: (a) Position of sting-jet precursor grid points (dots) within identified sting-jet precursor regions with respect to cyclone centres. The azimuth angle was measured with respect to instantaneous cyclone travel direction (C-axis). The shaded area represents the average precursor region (computed as described in section 2.2.2). (b) Frequency of sting-jet precursors as a function of the amount of CSI (as measured by maximum value of DSCAPE in a column), and (c) frequency of sting-jet precursors as a function of p^{*}_{top}. The 100 most intense cyclones in the North Atlantic during winter months from December 1989 to February 2009 are considered.

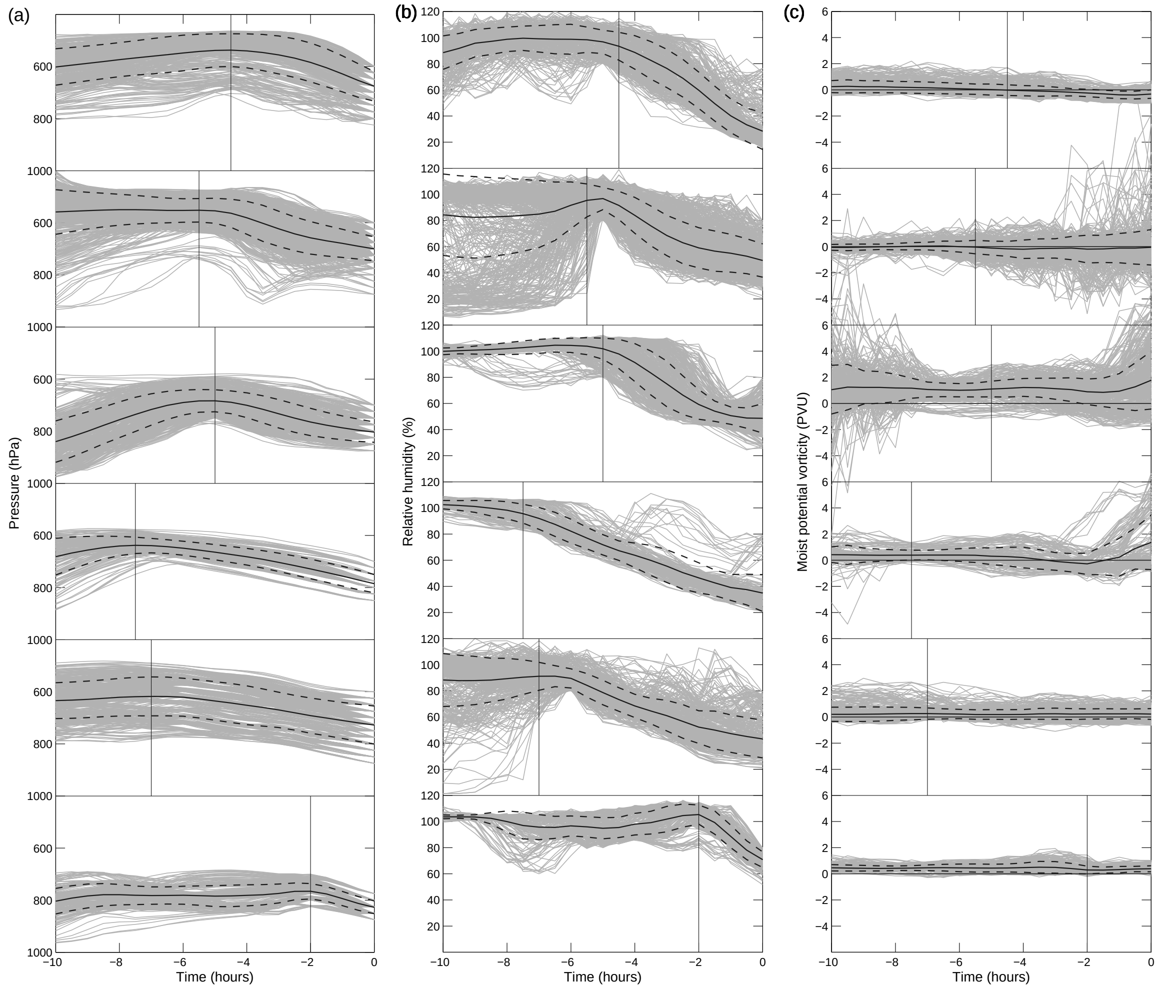

Figure 5: Trajectory analysis of the sting-jet cases found in the high-resolution simulations for (a) pressure, (b) RH and (c) MPV*, showing ensemble members (grey), ensemble mean (black solid) and ± one standard deviation from the mean (black dashed). Vertical lines mark the onset of the sting-jet descent. Each row corresponds to a different cyclone with time zero defined as follows: (1) 0700 UTC 6 December 1994, (2) 0700 UTC 18 December 1995, (3) 0000 UTC 28 December 1998, (4) 2100 UTC 10 December 2001, (5) 0800 UTC 5 December 2002 and (6) 1400 UTC 12 December 1994.